

Modeling the performance of coated LPG tanks engulfed in fires

Gabriele Landucci^a, Menso Molag^b, Valerio Cozzani^{c,*}

^a CONPRICI - Dipartimento di Ingegneria Chimica, Chimica Industriale e Scienza dei Materiali, Università di Pisa, via Diotisalvi n.2, 56126 Pisa, Italy

^b Nederlandse Organisatie voor toegepast-natuurwetenschappelijk onderzoek TNO, Princetonlaan 6, 3584 CB Utrecht, The Netherlands

^c CONPRICI - Dipartimento di Ingegneria Chimica, Mineraria e delle Tecnologie Ambientali, Alma Mater Studiorum - Università di Bologna, Via Terracini 28 - 40131 Bologna, Italy

ARTICLE INFO

Article history:

Received 28 April 2009

Received in revised form 7 July 2009

Accepted 8 July 2009

Available online 15 July 2009

Keywords:

Major accident hazard

Domino effect

BLEVE

Finite element modeling

Thermal protection

ABSTRACT

The improvement of passive fire protection of storage vessels is a key factor to enhance safety among the LPG distribution chain. A thermal and mechanical model based on finite elements simulations was developed to assess the behaviour of full size tanks used for LPG storage and transportation in fire engulfment scenarios. The model was validated by experimental results. A specific analysis of the performance of four different reference coating materials was then carried out, also defining specific key performance indicators (KPIs) to assess design safety margins in near-miss simulations. The results confirmed the wide influence of coating application on the expected vessel time to failure due to fire engulfment. A quite different performance of the alternative coating materials was evidenced. General correlations were developed among the vessel time to failure and the effective coating thickness in full engulfment scenarios, providing a preliminary assessment of the coating thickness required to prevent tank rupture for a given time lapse. The KPIs defined allowed the assessment of the available safety margins in the reference scenarios analyzed and of the robustness of thermal protection design.

© 2009 Elsevier B.V. All rights reserved.

1. Introduction

In the framework of liquefied petroleum gas (LPG) transportation and distribution, one of the more critical issues under the point of view of safety is related with the potential consequences of BLEVEs (boiling liquid expanding vapour explosions). This may be caused by the catastrophic rupture of LPG tanks, exposed to fires during the travel or during loading/unloading operations as a consequence of accidental events [1,2]. Data on past accidents obtained from specific databases demonstrated that among the more severe accidents occurred during the transportation of LPG by road or rail (95 records), more than 33% involved “fired”-BLEVEs [3]. Moreover, accident records evidenced that this scenario is likely to occur at loading/unloading facilities (such as refuelling stations) in vulnerable urban areas (24% of the total “fired”-BLEVEs accidents).

Hence, a key issue to enhance safety and to reduce the risks related to LPG transportation is the development and the application of protective measures, able to prevent or, at least, to delay for a time lapse sufficient for emergency response, the thermal collapse of the tank. The required time lapse can be assessed on the basis of standards and/or experience concerning the response times needed by emergency teams to reach the site of the accident and to start effective mitigation actions [4].

Data on several fire tests carried out and available in literature [5–8] pointed out that LPG tanks with no fire protection may withstand pool fire engulfment conditions for time lapses typically comprised between 5 and 25 min, depending on fire intensity and tank characteristics. Such a time lapse, in general, is not sufficient to assure the prevention of BLEVE scenarios by external mitigation actions in the case of road and rail transport accidents [4]. Protective measures as relief valves and fire protection by thermal coatings may hinder tank pressurization and tank wall heat-up, thus delaying and/or allowing the prevention of “fired” BLEVEs occurrence. The adoption of such measures is compulsory in several countries [1], but not in Europe, where the ADR [9] and the RID [10] standards allow respectively road and rail transportation of LPG in uncoated tanks.

Several issues are still open concerning the possible implementation of effective fire protections based on thermal coating for road and rail tankers in the specific European context. A wide uncertainty is present concerning the time lapse required for emergency response on road or rail accidents. This leads to the need for an accurate selection of the coating material and of the thickness of the coating layer, in order to enhance the available time lapse before tank failure, optimizing the costs due to the adoption of the protective measures.

Although several simplified models [11–21] and some more detailed approaches [22–24] were proposed in the literature for the calculation of the time to failure of LPG tanks engulfed by fires, scarce work was done to understand in detail the effects of protective coatings on the time to failure of pressurized tanks. In the

* Corresponding author. Tel.: +39 051 2090240; fax: +39 051 2090247.
E-mail address: valerio.cozzani@unibo.it (V. Cozzani).

Nomenclature

| | |
|----------------------|---|
| ADR | European agreement concerning the international carriage of dangerous goods by road |
| BLEVE | boiling liquid expanding vapour explosion |
| FEM | finite element model |
| KPI | key performance indicator |
| LPG | liquefied petroleum gas |
| MG | geometric mean bias |
| PRV | pressure relief device |
| RI | robustness index |
| RI* | reference value for the robustness index |
| RID | European agreement concerning the international carriage of dangerous goods by rail |
| S_{ins} | minimum coating thickness to avoid the vessel failure (mm) |
| SI | stress index |
| SI* | reference value for the stress index |
| t_m | reference time for effective mitigation (min) |
| t_R | reference time (min) |
| t_{tf} | time to failure (min) |
| T_1 | reference temperature for vessel shell weakening (°C) |
| T_2 | reference temperature for hydrocarbon flames (°C) |
| T_D | design temperature for real scale tanks (°C) |
| T_{exp} | measured temperature (°C) |
| T_f | temperature of a generic node at the end of simulation run (°C) |
| TI | temperature index |
| TI* | reference value for the temperature index |
| T_{mod} | temperature predicted by the model (°C) |
| VG | geometric variance |
| Greek letters | |
| $\Delta\sigma$ | residual stress margin (MPa) |
| σ_{adm} | maximum allowable stress or stress intensity limit (MPa) |
| σ_{eq} | stress intensity (MPa) |
| σ_{max} | maximum value of local stress intensity at the end of simulation (MPa) |

present study, an approach based on finite element modeling (FEM) was selected to explore the problem. A FEM developed in a previous study [25] was extended and further improved to allow the simulation of the protection offered by different types of coating in accidental fire scenarios. The model was validated using spe-

cific experimental data and was applied to analyze the behaviour, the failure modes and the time to failure of protected tanks in fire engulfment scenarios. In particular, the coating performance and the time to failure were assessed for road tankers, tank wagons and large scale storage vessels, obtaining data on the expected effectiveness of the protection.

2. The finite element model

2.1. Model set up

The model of real scale tanks engulfed by fire was based on a finite element approach summarized in Fig. 1. The FEM was implemented on the ANSYSTM software, using the ANSYSTM/Multiphysics module [26]. The basic approach used to develop the FEM was described in detail in a previous publication [25] and is only briefly outlined in the following.

The procedure to carry out the model runs may be divided in two parts: (i) thermal FEM, step 1 in Fig. 1; and (ii) mechanical FEM, step 2 in Fig. 1. The present approach, which allows assessing in a decoupled manner the thermal and hydraulic behaviour of fired tanks, is similar to the one used by Tan et al. [24]. This supports the validity of the applied methodology, and allows carrying out a detailed analysis.

The same geometry domain is implemented for both the analyses. In the case of cylindrical vessels, the calculation mesh was schematized as a uniform brick type, consisting in 6192 cells. For spherical tanks, the free mesh was preferred, and 6834 cells were defined. An overview of both geometry settings and meshes is reported in Fig. 2.

In step 1 (thermal FEM), the effect of radiation due to fire exposure, internal fluid behaviour and surface emissivity are the model inputs. The software carries out a thermal balance on the nodes, schematized in Fig. 3. Complicating effects related to the liquid temperature stratification and non-constant liquid level, which are extensively described in [27], are neglected. More details concerning the implementation of the thermal balance and thermal balance equations are reported elsewhere [25]. The outcomes of the thermal simulations are the detailed calculation of the temperature profiles on the vessel shell as a function of time and of radiation mode.

The second step of the modeling (step 2 in Fig. 1) is the simulation of the transient stress field as a function of the local temperatures and of the other loads present on the equipment shell. The transient evolution of the tank exposed to fire was simulated dividing the simulation total time in several stationary time steps (each 5 s real time) and applying a stress field analysis to each time step [26]. The results of the thermal simulations obtained in step 1 were implemented as thermal loads together with the other main

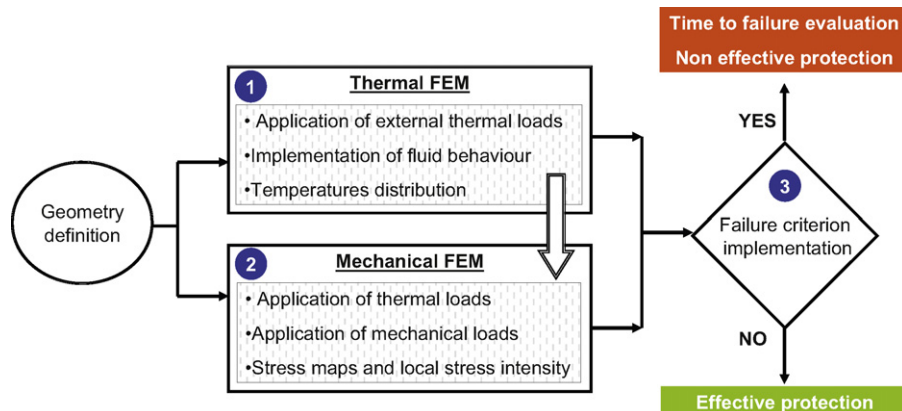


Fig. 1. Methodological approach used for FEM development.

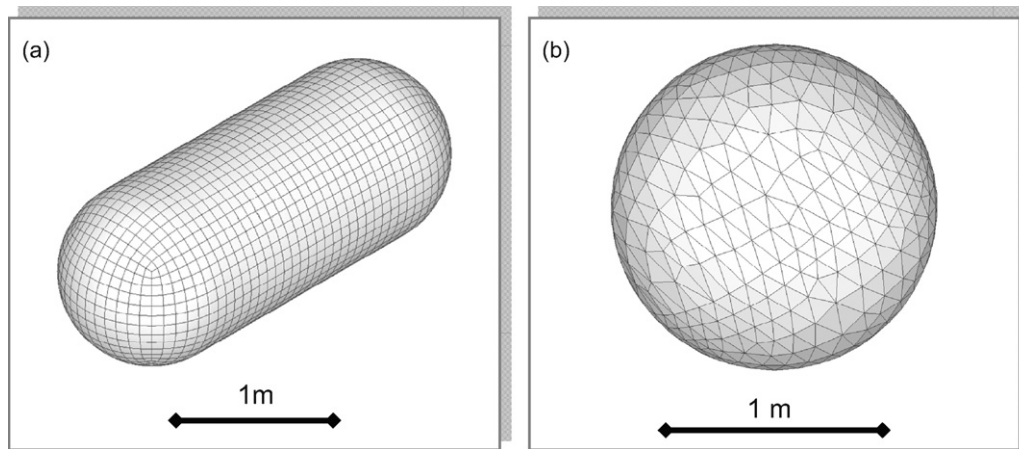


Fig. 2. Geometry and mesh definition for (a) horizontal cylindrical tanks and (b) spherical vessels, considered for model validation.

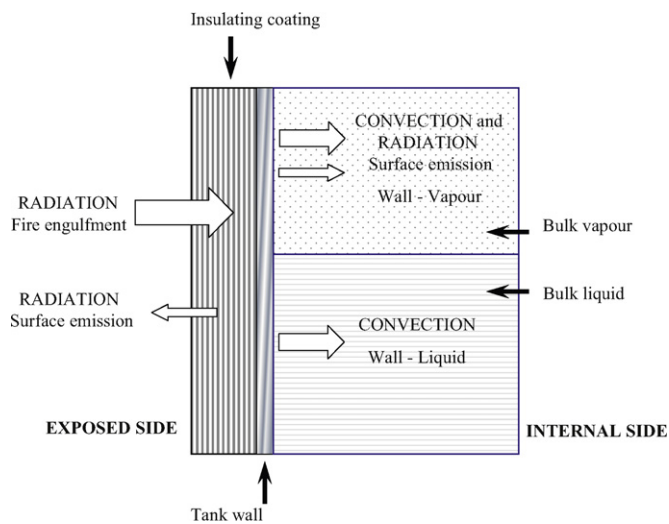


Fig. 3. Energy balance and boundary conditions used in the thermal FEM.

“mechanical” loads (weight, internal vapour pressure and hydrostatic pressure) to step 2. The distribution of the equivalent intensity of combined stress [28,29], in the following indicated as the stress intensity (labelled as σ_{eq}), was calculated. The stress intensity was then compared to a maximum allowable value, σ_{adm} . Data provided by Section VIII, Division 2 of ASME codes [28] were used to obtain a relation between σ_{adm} and the temperature, thus a temperature-dependent maximum allowable stress value was considered in the analysis.

The time to failure, t_{tf} , was defined as the minimum value of time since the start of the simulation run at which at least in one point of the calculus domain, the following equivalence is verified:

$$\sigma_{eq} = \sigma_{adm} \quad (1)$$

Table 1
Physical properties assumed for the reference fire proofing materials.

| Coating characteristics | Type 1 | Type 2 | Type 3 | Type 4 |
|------------------------------|-------------------|-----------------------|----------------------|------------------------------------|
| Definition | Epoxy intumescent | Vermiculite spray | Fibrous mineral wool | Cementitious inorganic formulation |
| Thermal conductivity (W/m K) | 0.066 | 0.03–0.2 ^a | 0.38 | 0.9 |
| Heat capacity (J/kg K) | 1172 | 970 | 920 | 1507 |
| Surface emissivity | 0.9 | 0.9 | 0.9 | 0.9 |
| Density (kg/m ³) | 1000 | 680 | 100 | 850 |

^a Low value for thicknesses greater than 35 mm; high value for thicknesses lower than 35 mm.

The plasticity region, associated to material residual strength, or the eventual creep arising, were thus not considered in the model, obtaining conservative results.

2.2. Modeling of thermal coatings

The implementation of the thermal coating in the FEM development is a crucial point for the thermal simulations (step 1). In the present analysis specific approaches were introduced to model the four type of coatings considered: (i) epoxy intumescent; (ii) vermiculite spray; (iii) fibrous mineral wool; and (iv) cementitious inorganic materials.

In the case of the two latter materials, constant thickness and average physical properties were supposed, neglecting thermal degradation effects that may follow the exposure to fire. In the case of epoxy intumescent coatings, the coating was supposed to expand instantaneously up to the final thickness, while constant properties were assumed during the simulation, neglecting the increase in the thermal conductivity that was experimentally verified for some intumescent coatings [30]. A uniform geometry and constant properties in simulation runs were thus obtained by these assumptions.

In the case of vermiculite sprays, a different approach was necessary. These coating materials exploit the water content to limit the temperature of the non-exposed side [31]. Water evaporation keeps the temperature to a constant plateau (close to the saturated steam temperature) for a time that depends on the coating thickness, which is related to the water content [31,32]. Experimental data evidenced that the minimum required thickness necessary for the activation of this behaviour is of 35 mm [31–33]. Thus, for a coating thickness equal or higher than 35 mm, an effective thermal conductivity function was used. The function is reported in Table 1 and was obtained from experimental data fitting. For a thickness lower than 35 mm, an average thermal conductivity value was considered for the material, as in the case of fibrous mineral wool and cementitious inorganic coatings.

Table 2
Data used for the validation of FEM.

| | Test ID | | | | |
|--|-------------------|-------------------|-------------------|-----------------------|---------------------|
| | EXP1 | EXP2 | EXP3 | EXP4 | EXP5 |
| | [32] ^a | [32] ^a | [32] ^a | [25] ^a | [34] ^a |
| Tank specifications | | | | | |
| Tank geometry | Spherical | Spherical | Spherical | Horizontal cylinder | Horizontal cylinder |
| External diameter (m) | 1.7 | 1.7 | 1.7 | 1.25 | 1.25 |
| Total length (m) | – | – | – | 2.68 | 4.3 |
| Minimum wall thickness (mm) | 10 | 10 | 10 | 5.1 | 6.4 |
| Filling level (%) | 20 | 20 | 20 | 50 | 20 |
| Type of material | Low carbon steel | Low carbon steel | Low carbon steel | Low carbon steel | Low carbon steel |
| Pressure relief device nominal diameter (mm) | – | – | – | 32 | 32 |
| Opening gauge pressure (MPa) | 1.6 | 1.6 | 1.6 | 1.46 | 1.46 |
| Insulating coating properties | | | | | |
| Coating type | Intumescent | Mineral cement | Mineral cement | Intumescent | Rock wool |
| Applied thickness (mm) | 10 | 38 | 35 | 10 | 100 ^b |
| Data on stored material | | | | | |
| Type | Propane | Propane | Propane | LPG grade A | Propane |
| Average liquid temperature (°C) implemented in FEM | 45 | 45 | 45 | 65 | 45 |
| Vapour temperature (°C) implemented in FEM | 250 | 99 | 90 | 287 | 150 |
| External heat source | | | | | |
| Exterior temperature (°C) | 29 | 20 | 22 | 12 | 25 |
| Type of fire | Engulfing burners | Engulfing burners | Engulfing burners | Pool fire (3 m × 6 m) | Surrounding fire |
| Thermal load in simulations (kW/m ²) | 186.7 | 173 | 177 | 130 | 170 |

^a Data source.

^b Coating was encapsulated in a watertight steel sheet coating 1 mm thick; 30 mm air gap was left between the sheet and the coating.

2.3. Model validation

The FEM was validated against experimental results obtained in bonfire tests on thermally insulated tanks [25,32,34]. Computer simulations were performed to simulate the field tests reported in Table 2. Test conditions, features and sizes of the tanks are also summarized in the table, in which the key parameters for the FEM simulations are reported. More details on the coating material properties are reported in Table 1.

For the sake of brevity, only two examples of detailed comparison between the experimental results and the model predictions are reported in Fig. 4. Data are referred to the maximum wall temperature (e.g. the tank shell section in contact with the vapour phase) obtained from EXP1 and EXP2 (see Table 2 for details). In these tests, spheres for propane storage, having a 2.5 m³ capacity, were totally engulfed in fire. The heat source reproduced a butane pool fire with different burner-banks distributed among the sphere surface. Considering the maximum flame temperature for the two tests, the thermal load on the coating was calculated assuming the flame as a blackbody, thus obtaining the values reported in Table 2.

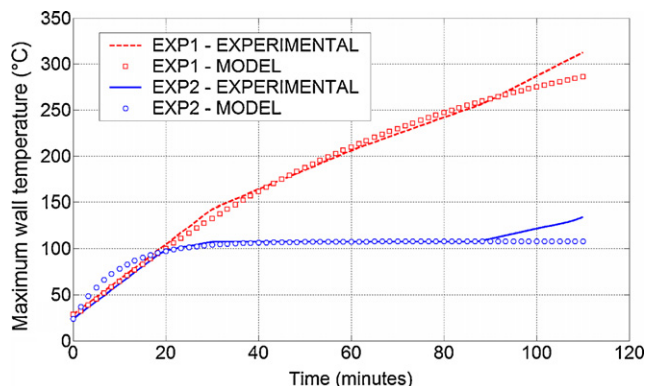


Fig. 4. Comparison between experimental and model temperatures for tests EXP1 and EXP2. Temperatures in °C. End of simulation: 110 min.

In EXP1, a commercial intumescent coating was used. Therefore, the coating expansion was considered, following the indications reported in Section 2.1. As shown in the figure, a good agreement is present between experimental data and model predictions, up to about 95 min from the beginning of the test. In the final part of the run, however, the model under-predicts the actual wall temperatures of about 30 °C, with a relative error of about 10%. This error may be caused by model limitations in the simulation of coating behaviour: in particular, on the basis of supplier indications [25], constant properties were used for the coating layer, and a uniform behaviour of the protection coating was assumed, without considering the coating consumption due to fire exposure.

In EXP2, a commercial mineral coating, based on a vermiculite spray, was used. In this case, supposing an initial thickness of 38 mm, the water loss was considered. As shown in Fig. 4, in the first part of the run the wall temperature presents a plateau at 100 °C, lasting about 1 h, well predicted by the model runs. The use of the effective thermal conductivity values reported in Table 1 allows a sufficiently accurate assessment of the behaviour of the mineral cementitious coating material, with a small average relative error (6%). Also in this case the coating degradation was not considered in the model. This is the likely cause of the under-prediction of the temperature in the final part of the run (a maximum temperature difference of 26 °C is present, as shown in Fig. 4).

The method proposed by Hanna et al. [35] was used to analyze model performance in wall temperature prediction. The model is based on the calculation of the geometric mean bias (MG), the geometric variance (VG), of measured and predicted values:

$$MG = \exp \left[\overline{\ln(T_{exp})} - \overline{\ln(T_{mod})} \right] = \exp \left[\ln \left(\frac{T_{exp}}{T_{mod}} \right) \right] \quad (2)$$

$$VG = \exp \left[\overline{(\ln(T_{exp}) - \ln(T_{mod}))^2} \right] = \exp \left[\left(\overline{\ln \left(\frac{T_{exp}}{T_{mod}} \right)} \right)^2 \right] \quad (3)$$

where T_{exp} is the measured temperature and T_{mod} is the temperature predicted by the model at the reference time of interest. The over-bars indicate that an average is performed over the data set.

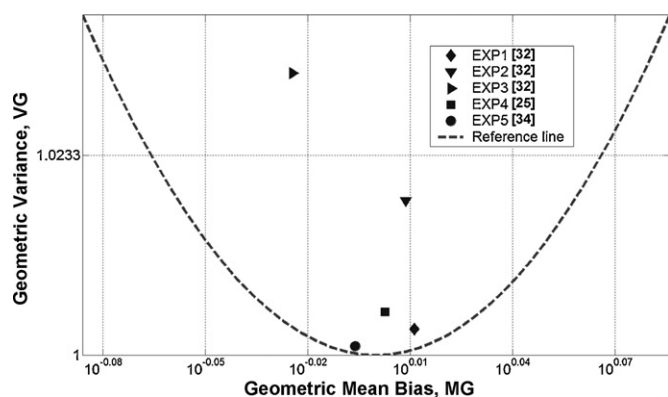


Fig. 5. Geometric mean bias (MG) and geometric variance (VG) for model simulations compared to experimental results as defined by Eqs. (2) and (3). Dashed line: reference parabola defined in Eq. (4).

Good model performances are achieved when both MG and VG are close to unity. In order to allow a systematic performance assessment, VG values may be plotted vs. the corresponding MG values for each data set and may be compared to the following reference parabola:

$$\ln(VG) = (\ln(MG))^2 \quad (4)$$

As evident from Eqs. (2) and (3), Eq. (4) represents the correlation among VG and MG values in a model having only a mean bias with respect to experimental data (that is, a model in which the ratio of T_{exp}/T_{mod} is nearly constant), but showing no systematic deviations. Thus, models having a good performance and showing no systematic deviations should provide VG values that fall on or above the correlation curve given by Eq. (4).

Fig. 5 reports the reference curve from Eq. (4) and the VG and MG data calculated for the maximum wall temperature values predicted in the different model simulations. As shown in the figure, all the spots calculated are above the correlation curve and are quite close to unity. The best results are obtained in the case of epoxy intumescent coatings (EXP1 and EXP4), which, however, present a slight underestimation of temperature due to coating degradation in the final part of the test. Data obtained for vermiculite sprays (e.g. EXP2 and EXP3) present slightly higher values of VG . Data obtained for EXP5 result in a VG value very close to unit, also showing a good model performance.

Therefore, both error analysis and statistical indicators show that the model is able to successfully predict the values of wall temperatures for coated tanks in bonfire experiments. Thus, the model was applied to analyze the real scale case studies of interest in the present study.

3. Definition of case-studies

The approach developed was applied to assess the performance of thermal coatings in the protection of LPG tanks in the framework of the LPG distribution chain. In particular, a set of case studies of

interest was defined, considering both storage tanks used in fixed installations and for LPG road and rail transport. Three horizontal cylindrical vessels were considered:

- Reference vessel #1: 60 m³ tank for road LPG transportation;
- Reference vessel #2: 110 m³ tank for rail LPG transportation;
- Reference vessel #3: 220 m³ fixed bulk storage tank.

The vessels were selected in order to represent reference tank geometries typically used in the applications considered. Table 3 summarizes the main geometrical data assumed for the tanks. Reference sizes of trailer tanks complying to European ADR and RID standards were selected [9,10]. ASME standards [28] were used to select the wall thickness of reference vessel #3. The pressure relief devices (PRV) were sized following the guidelines provided by API RP521 standard. A low carbon steel (DIN 17102 St E460 grade) was considered as the building material of all the tanks. A 50% filling level was assumed for all reference tanks.

Past accident analysis was used to identify and select the more significant fire scenarios leading to tank catastrophic failure for each type of reference tank considered. A thorough analysis of BLEVE case-histories reported in the MHIDAS database [3] was carried out. For all the three reference tanks full engulfment in a pool fire was assumed as a conservative reference accidental scenario. In the case of road accidents, this may be caused by the release and ignition of diesel fuel due to engine damage in the accident. In the case of rail accidents, the pool fire may be caused by the damage of nearby tank cars carrying flammable liquids. In the case of fixed tanks this may arise from the late ignition of LPG released from tank connections.

The characterization of the scenarios allowed the estimation of the thermal load on the vessel due to fire impingement in each scenario (see Section 2.1) [4,36]. The quantification of the net thermal load was based on available experimental data for large pool fires [37,38]. The results of this preliminary assessment are summarized in Table 4. The thermal coatings described in Section 2.2 were considered for real scale simulations. The detailed properties assumed for the coatings are reported in Table 1. Different thicknesses were implemented in the analysis, ranging from 5 to 100 mm. Simulations runs were carried out as for the unprotected tanks.

4. Results and discussion

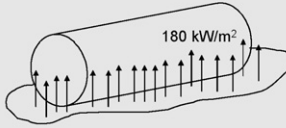
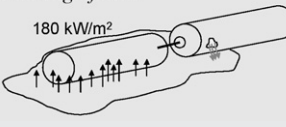
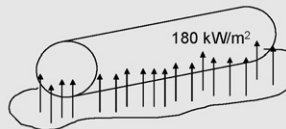
4.1. Vessel temperature and stress maps

In Fig. 6a an example of wall temperature distribution is reported for reference vessel #1. A 40 mm thick fibrous mineral wool coating (type 3) was considered, encapsulated in a watertight steel sheet coating, with a 30 mm air gap between the sheet and the coating. The tank is sectioned among the axis in order to show temperature distributions on both internal and external surfaces. The figure shows the temperature map of the inner tank wall at different times since the beginning of the fire. As shown in the figure, higher inner wall temperatures are present on the wall section in contact with the vapour phase, due to the low heat transfer coefficients between

Table 3
Data assumed for the three reference tanks used in model runs.

| Item | Reference vessel #1 (road tanker) | Reference vessel #2 (tank wagon) | Reference vessel #3 (large scale storage) |
|--------------------------------------|-----------------------------------|----------------------------------|---|
| Nominal volume (m ³) | 60 | 110 | 220 |
| Diameter (m) | 2.4 | 3.04 | 3.35 |
| Length (m) | 13.5 | 16.04 | 27.43 |
| Minimum wall thickness (mm) | 12.2 | 31 | 31 |
| Working pressure (MPa) at 25 °C | 0.5 | 0.5 | 0.5 |
| Design gauge pressure (MPa) | 1.82 | 2.4 | 1.6 |
| PRV discharge area (m ²) | 0.004 | 0.005 | 0.01 |

Table 4
Reference scenarios associated to the three reference tanks.

| Reference tank | Fire scenario | Fire attack conditions | Range of thermal loads (kW/m ²) |
|---|--------------------------|---|---|
| Reference tank #1 (road tanker) | Naphtha/diesel pool fire | Full engulfment  | 100–180 |
| Reference tank #2 (tank wagon) | Hydrocarbon pool fire | Full engulfment  | 100–180 |
| Reference tank #3 (large scale storage) | LPG pool fire | Full engulfment  | 150–250 |

the wall and the vapour. However, the maximum wall temperature value never exceeds 470 °C, even after 100 min of exposition to fire. The wall section in contact with the liquid presents lower temperatures that show a very limited increase during the simulation. Strong temperature gradients are present on the structure, since for the entire simulation the heat load applied leads to an almost constant peak temperature of 1130 °C on the surface of the external coating in contact with the flame.

The results of thermal FEM were implemented in the mechanical FEM (see Fig. 1) to calculate the stress intensity distribution. Fig. 6b reports the stress maps calculated on the basis of the temperature distributions reported in Fig. 6a. As shown in the figure, during the simulation the structure experiences an increasing internal pressure (due to vapour pressure increase) and an increasing

temperature, which result in higher stresses among the entire tank wall. The stress intensity strongly increases in the upper part of the vessel, due to the effect of higher temperatures in contact with the vapour phase.

A second critical zone is in correspondence of the liquid/vapour interface. In this zone, the model predicts the highest stress intensity values among the structure, due to the strong temperature difference between the upper and the lower part of the tank. As shown in Fig. 6a, a temperature difference of about 400 °C is present in the vessel inner wall temperature between the area of the vessel shell in contact with the vapour and the part of the vessel wall in contact with the liquid. This causes strong local stresses due to differences in thermal dilatation between the two parts of vessel shell (see Fig. 6b). As a matter of fact, in several past accidents as well

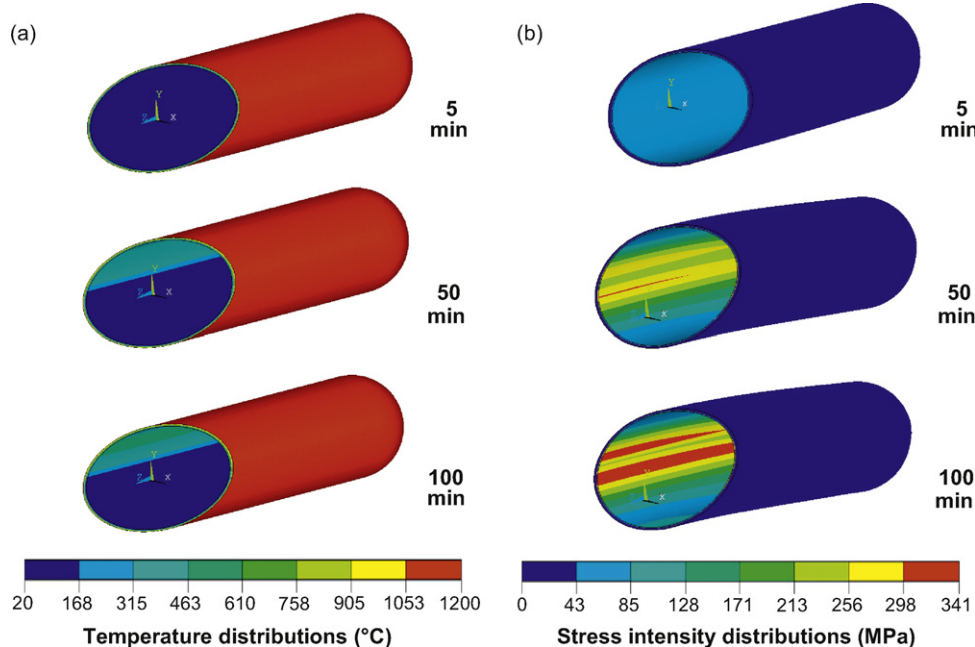


Fig. 6. Temperature maps (a) and stress intensity distributions (b) on reference vessel #1 during fire engulfment (180 kW/m² heat load) at different simulation run times (5, 50 and 100 min). Type 3 coating: 40 mm thick rock wool.

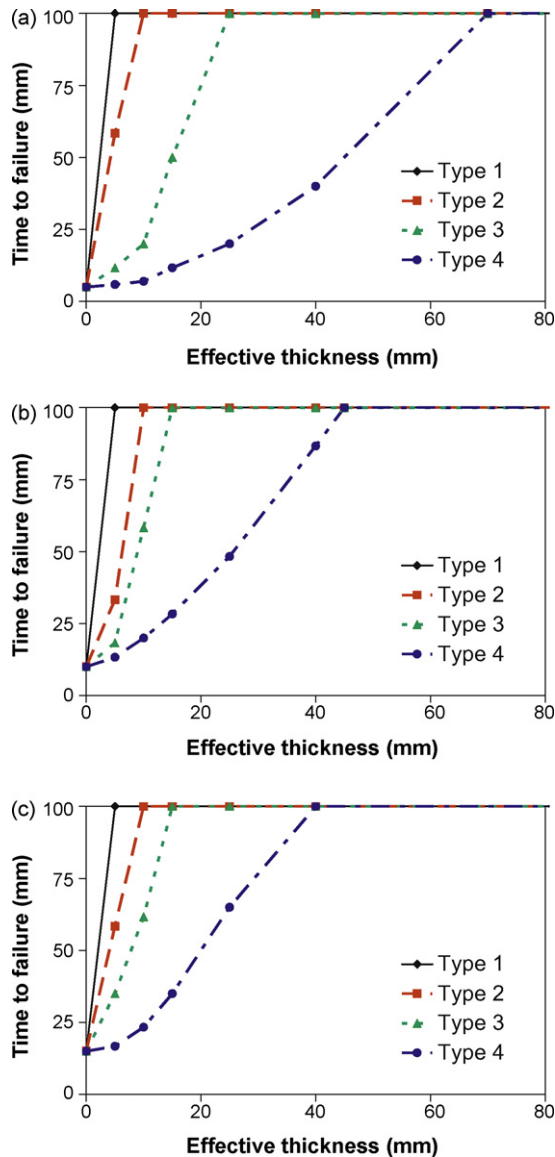


Fig. 7. Time to failure (min) as a function of coating effective thickness (mm) and of coating type for: (a) reference vessel #1 (60 m³ road tanker); (b) reference vessel #2 (110 m³ tank wagon); and (c) reference vessel #3 (220 m³ large scale storage). Fire scenario: 180 kW/m² constant heat load.

as in experiments the rupture of tanks exposed to fires was experienced at the liquid/vapour interface [6,32]. These results clearly show the advantages of a detailed analysis, which allows taking into account phenomena that are neglected by simplified criteria based on maximum wall temperatures that are proposed for a preliminary assessment of the possibility of tank failure [39,40].

4.2. Optimal design of thermal protections

The simulations carried out on large scale tanks were aimed at demonstrating the effectiveness of the thermal coatings in preventing the structural damage of tank shell, and/or a catastrophic tank rupture following fire engulfment. Fig. 7 reports the variation of time to failure for different tank geometries, coating materials and coating thicknesses. The simulations were carried out for a maximum reference time t_R of 100 min. As shown in the figure, coating type 1 was the only category of material which allowed preventing the failure of the tank up to the reference time t_R in all the scenarios considered. This is due to the extremely low thermal conductivity

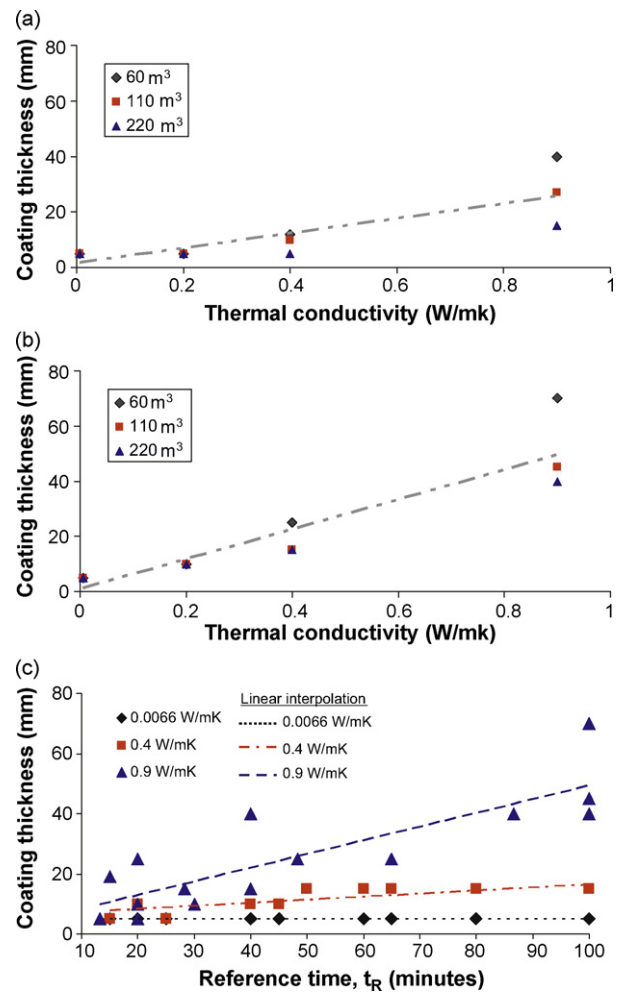


Fig. 8. Minimum coating thickness (mm) needed to avoid tank rupture as a function of the thermal conductivity of the coating (W/mK). Fire scenario: 180 kW/m² constant heat load; 60, 110 and 220 m³ vessels. (a) Coating thickness vs. thermal conductivity, reference time 30 min; (b) coating thickness vs. thermal conductivity, reference time 100 min; (c) minimum coating thickness (mm) vs. reference time (min) as a function of the thermal conductivity (W/mK).

of the coating material that is about an order of magnitude lower than that of the other coatings considered. However, it should be remarked that changes of thermal conductivity during fire exposition were not considered in the model.

Coating types 2 and 3 also showed good performances, preventing the tank failure in the reference time for thicknesses higher than 10 mm. Nevertheless, it appears that the lower “thermal inertia” (e.g. the effect of the small density of coating type 3) affects negatively the effectiveness of the protection. In the case of type 4 coating, the results are drastically worse than those of the other materials. This is due to the higher thermal conductivity, which causes a higher temperature rise.

A preliminary indication for fireproofing design may be obtained from the analysis of the minimum thickness of each coating, s_{ins} , needed to avoid the rupture before reference time t_R considering the application of different coating materials. The thermal conductivity of the coating was identified as the key parameter for the characterization of a fire proofing material. Fig. 8 shows the calculated minimum coating thickness s_{ins} reported as a function of the reference time, t_R , for different tank geometries and coating types. It is obvious that an increase in the coating performance directly results in a reduction of the required thickness, s_{ins} . This effect is amplified for higher values of t_R , as confirmed by the increase in the slope of the interpolating curve in Fig. 8b with respect to the

Table 5

Key performance indicators defined to assess the robustness of thermal protection design (*ttf*: time to failure; *tm*: reference time for effective mitigation; T_1 : reference temperature for vessel shell weakening, °C; T_2 : reference temperature for hydrocarbon flames, °C).

| KPI | Symbol | Definition | Reference value |
|-------------------|-----------|-------------|-----------------|
| Robustness index | <i>RI</i> | ttf/tm | 1 |
| Temperature index | <i>TI</i> | T_1/T_2 | 0.36 |
| Stress index | <i>SI</i> | See Eq. (6) | 0.33 |

one in Fig. 8a. This issue is further evidenced in Fig. 8c that shows the minimum thickness, s_{ins} , as a function of reference time t_R for different thermal conductivities corresponding to different coating types.

The geometry of the vessel plays an important role only in the case of higher values of thermal conductivity, with a higher thickness needed as the tank volume decreases. On the contrary, in the case of more performing coating materials, the protection appears effective in all the scenarios considered and shows a limited dependence from geometry (see Fig. 8a and b).

4.3. Key performance indicators for thermal protection robustness

In the above discussion, the results of FEM simulation were only used to assess tank failure conditions. However, the results of the FEM may also yield important information on the expected performance of the coating and, in particular, on the robustness of the design of thermal protections. Three key performance indicators (KPIs) were introduced to obtain an assessment of the robustness and the safety margins available for a specific thermal protection design. The three KPIs defined are listed in Table 5. As shown in the table, the KPIs are based on calculated values obtained from FEM simulations for the time to failure, the vessel shell temperatures and the vessel shell stresses. The table also reports a safety reference value for each KPI that may be considered as a blue line for a robust protective action (see Table 5).

The first KPI, labelled as *RI*, was defined as the ratio between the calculated time to failure, *ttf*, for a specific fire scenario (full engulfment) and a reference time of interest, t_R . This was assumed equal to the maximum time required to start effective mitigation actions, *tm*, likely to prevent the BLEVE of the vessel. Further details on the definition and on the assessment of site-specific values for the time required for effective mitigation are reported elsewhere [29]. In the present study, a value of 100 min was assumed for *tm* in the case of reference vessels #1 and #2 (fire scenarios involving road or rail accidents) [4], and a value of 30 min was assumed for reference vessel #3 (fixed installation) [29,39].

The *RI* may be interpreted as a robustness index that provides a quantitative assessment of the time lapse still available with respect to failure condition following fire exposure in the reference scenarios considered. The reference value of this KPI is obviously equal to 1 (that means that the *ttf* equals the maximum time for effective mitigation). Values of *RI* below 1 define an “unsafe” region, where tank failure may be expected even in the presence of the coating, since the protection provided may not be sufficient to allow the start of mitigation actions.

The second KPI defined, labelled as *TI*, is based on the assessment of vessel shell temperature gradients. The *TI* index is defined as the ratio between the maximum temperature reached by the inner surface of tank wall and the maximum temperature of the external coating surface at a reference time of interest, t_R . The reference time of interest should be selected as the time for effective mitigation, *tm*, or the time to failure, *ttf*, if the latter has a lower value.

A blue-line reference value for *TI* may be defined as the ratio of two significant temperatures, the first representing a reference value for the thermal weakening of the vessel shell material, the sec-

ond representing the typical temperature of flames in hydrocarbon fires. According to the indications reported in literature [39,40] a value of 400 °C may be assumed for the first reference temperature, T_1 , in the case of steel vessels. The second reference temperature, T_2 , may be derived from the standard fire curve which describes the transient evolution of a hydrocarbon fire (see [40] for more details). A value of 1100 °C may be assumed that corresponds to the steady-state temperature according to the fire curve. Since it is reasonable that the temperature of the outer coating surface is close to that of the flame in full engulfment scenarios [40], it is clear that a temperature gradient lower than that defined above identifies an unsafe region where tank failure may start. Thus, *TI* values lower than the reference value define an unsafe region where tank shell failure becomes possible.

The third KPI considered, *SI*, was defined as the ratio between a reference value for the residual allowable stress at a reference time of interest, t_R , and the maximum allowable stress in the absence of fire. Again, the reference time of interest, t_R , may be assumed as the time for effective mitigation, *tm*, or the time to failure, *ttf*, if the latter has a lower value. The residual stress margin at time t_R , $\Delta\sigma$, may be calculated as:

$$\Delta\sigma = \sigma_{adm}(T_f) - \sigma_{max}(t_R) \quad (5)$$

where $\sigma_{adm}(T_f)$ is the maximum allowable stress at the final temperature of the run, T_f , and $\sigma_{max}(t_R)$ is the maximum value of local stress intensity at time t_R . Being $\sigma_{adm}(T_D)$ the maximum allowable stress at the design temperature, T_D , the *SI* index may thus be expressed as follows:

$$SI = \frac{\Delta\sigma}{\sigma_{adm}(T_D)} \quad (6)$$

Clearly enough, the *SI* index should be evaluated in the more critical point of the structure that is the one where the local stress is higher. In this condition, the *SI* index expresses how far the vessel shell is from the failure conditions at the reference time of interest. The value of the index equals 0 if vessel rupture is predicted.

In order to provide a reference value for the *SI* index, the factor used in ASME section VIII standards [28] to derive the stress intensity design limit was taken into account. In particular, the stress intensity limit is obtained by reducing the tensile yield of the material by a factor 1.5. Hence, a safety margin equal to the 33% of the tensile yield is considered between the stress intensity limit and the tensile yield itself in design conditions. Therefore, 0.33 is assumed as a reference value for the *SI* index. The region where the values of *SI* become lower than 0.33 is therefore considered an “unsafe” zone, where vessel integrity is jeopardised.

Fig. 9 reports the values calculated for the KPIs considering a full engulfment scenario, the reference tanks defined in Section 3, the four coating materials listed in Table 1, and three coating thicknesses: 10, 25 and 40 mm. The same reference times assumed for *RI* index, e.g., 100 min for reference vessels #1 and #2 and 30 min for reference vessel #3, were also considered in the calculation of *SI* index.

In Fig. 9a, the values calculated for *RI* were plotted as a function of *TI* for several simulation runs performed. In the case of simulations which did not result in tank rupture, the *RI* index is equal to 1. For the thicknesses considered, coating types 1 and 2 always resulted in unit values of the *RI* index, due to their low thermal conductivity resulting in high performances.

Nevertheless, some of the scenarios in which *RI* is equal to 1 show values of the temperature index exceeding the safe reference value, TI^* . These spots fall into an “unsafe zone” (the red region in Fig. 9a), where the coating may not prevent the wall material weakening due to high temperatures. Quite obviously, all the spots having a non-unitary *RI* (thus the runs for which tank failure was predicted) fall all inside the unsafe region.

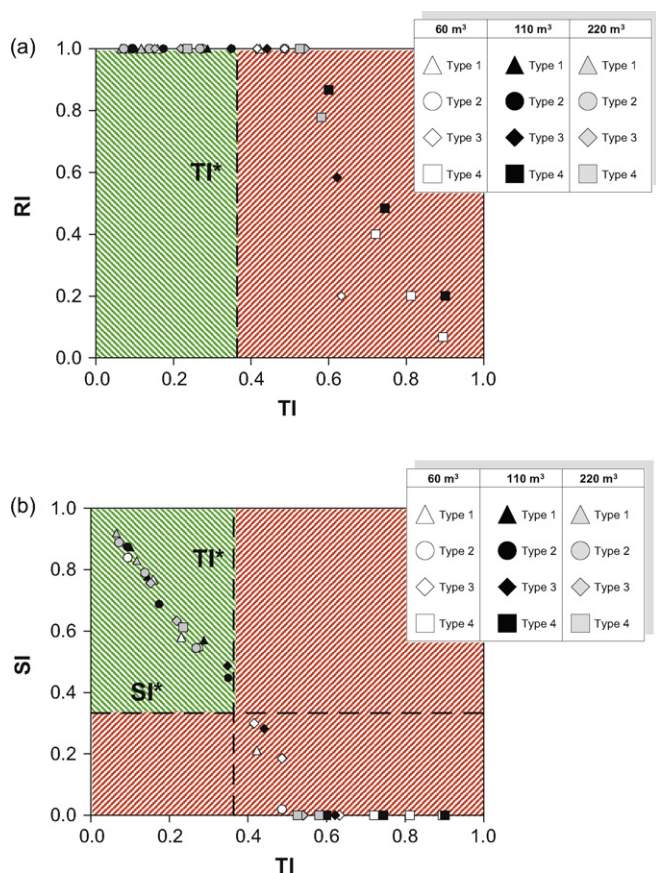


Fig. 9. Comparison among the KPIs calculated for different thermal protection systems: (a) robustness index (RI) vs. temperature index (TI); (b) stress index (SI) vs. temperature index (TI) for the three types of reference vessels. Green and red background identify “safe” and “unsafe” regions respectively. RI^* , TI^* , SI^* : reference values for KPIs reported in Table 5 (For interpretation of the references to color in this figure legend, the reader is referred to the web version of the article).

As shown in Fig. 9a, an increase of the TI index always corresponds to a decrease of RI which approaches 0 in the case of coating type 4. Moreover, the geometry strongly affects the results. As shown in Fig. 9a, the number of spots in the unsafe zone decrease with the increase in the size of the tank. This is due to the higher wall thickness coupled to a different design pressure and thickness/diameter ratio of larger tanks (110 and 220 m³), which enhances the resistance of the structure [28].

Fig. 9b reports the stress index SI as a function of temperature index TI , calculated for the same scenarios shown in Fig. 9a. The SI is particularly influenced by the vessel shell temperature that affects the steel residual strength. Thus, SI is strictly dependent on the TI index, as shown by the linear trend of the spots in Fig. 9b. Also in this case, the reference values defined identify an unsafe zone (the red region in Fig. 9b), where residual strength is below the usual design safety margins. The lower performance of coating types 3 and 4 is evident from the figure, even for the high thicknesses considered. Coating types 1 and 2 present both only one spot in the unsafe zone when the lower thickness is considered (10 mm).

Thus, the calculation of the KPIs allowed the assessment of the robustness of design of thermal protections. On one hand, as shown in Fig. 9, even if no failure is predicted, “unsafe” regions may be identified, where a detailed assessment of the effectiveness of thermal protection design needs to be carried out for the specific fire scenarios of concern. On the other hand, KPI values below the safe reference values defined are indicators of a robust design for the fire scenario considered in the assessment.

5. Conclusions

A numerical approach based on FEM was developed to assess the behaviour of LPG tanks engulfed by fires. The model developed was applied to investigate the performance of different materials proposed for the passive fire protection of tanks. A specific methodology, based on key performance indicators, was developed to allow an effective screening of alternative coating materials.

The results confirmed on one hand the wide influence of coating application on the expected time to failure. On the other hand, the comparison of the KPIs evidenced a quite different performance of the alternative materials proposed. In particular, organic intumescent and vermiculite sprays resulted in better performances due to inherent thermal properties, which limit the vessel shell heating for extended time lapses. Conventional fibrous mineral wool or cementitious inorganic formulations appeared not effective in some scenarios considered, allowing a stress increase among the vessel shell, combined with the material wall weakening due to high temperatures.

On the basis of the results obtained, general correlations were developed among the vessel time to failure and the effective coating thickness in full engulfment scenarios, providing a preliminary assessment of the coating thickness required to prevent tank rupture for a given time lapse. Indications on safety margins required to obtain a robust design were also provided by a specific set of KPIs.

References

- [1] M. Molag, A. Kruihof, BLEVE prevention of a LPG tank vehicle or a LPG tank wagon, Report R2005/364, Netherlands Organisation for Applied Scientific Research—TNO, Apeldoorn, 2005.
- [2] M. Molag, Product-chain-analysis ammonia, chlorine and LPG, phase 1 technical, components, economical and external safety aspects in the chain (in Dutch), Report R2003/205, Netherlands Organisation for Applied Scientific Research—TNO, Apeldoorn, 2003.
- [3] OSH-ROM, HSELINE, C15DOL, MHIDAS, NIOSHTIC, Silver Platter, London, 1998.
- [4] J.F.A. Hobert, M. Molag, Fire brigade response and deployment scenarios to avoid a hot BLEVE of a LPG tank vehicle or LPG tank wagon, Report 2006-A-R0069/B, Netherlands Organisation for Applied Scientific Research—TNO, Apeldoorn, 2006.
- [5] W. Townsend, C.E. Anderson, J. Zook, G. Cowgill, Comparison of the thermally coated and uncoated rail tank-cars filled with LPG subjected to a fire environment, Report FRA-OR&D 75-32, US Department of Transportation—DOT, 1974.
- [6] D. Kielec, A.M. Birk, Analysis of tank deformation from fire induced ruptures and BLEVEs of 400 L propane tanks, ASME J. Press. Technol. 119 (1997) 365–373.
- [7] M.A. Persaud, C.J. Butler, T.A. Roberts, L.C. Shirvill, S. Wright, Heat-up and failure of Liquefied Petroleum Gas storage vessel exposed to a jet-fire, in: Proceedings of 10th Int. Symp. on Loss Prevention in the Process Industries, Stockholm, 2001, pp. 1069–1106.
- [8] A.M. Birk, D. Poirier, C. Davison, On the response of 500 gal propane tanks to a 25% engulfing fire, J. Hazard. Mater. 19 (2006) 527–541.
- [9] Directive 2006/89/EC of 3 November 2006 adapting for the sixth time to technical progress Council Directive 94/55/EC on the approximation of the laws of the Member States with regard to the transport of dangerous goods by road.
- [10] Directive 2006/90/EC of 3 November 2006 adapting for the seventh time to technical progress Council Directive 96/49/EC on the approximation of the laws of the Member States with regard to the transport of dangerous goods by rail.
- [11] K.W. Graves, Development of a computer model for modeling the heat effects on a tank car, FRA-OR&D 75-33, 1973.
- [12] K. Moodie, Experiments and modelling: an overview with particular reference to fire engulfment, J. Hazard. Mater. 20 (1988) 149–175.
- [13] G.V. Beynon, L.T. Cowley, L.M. Small, I. Williams, Fire engulfment of LPG tanks: heat-up a predictive model, J. Hazard. Mater. 20 (1988) 227–238.
- [14] A.M. Birk, Modelling the response of tankers exposed to external fire impingement, J. Hazard. Mater. 20 (1988) 197–225.
- [15] P.K. Ramskill, A description of the “Engulf” computer code—codes to model the thermal response of an LPG tank either fully or partially engulfed by fire, J. Hazard. Mater. 20 (1988) 177–196.
- [16] A.M. Birk, I.R.M. Leslie, State of the art review of pressure liquefied gas container failure modes and associated projectile hazards, J. Hazard. Mater. 28 (1991) 329–365.
- [17] A.M. Birk, Scale effects with fire exposure of pressure-liquefied gas tanks, J. Loss Prev. Proc. Ind. 8–5 (1995) 275–290.
- [18] M.R. Johnson, Tank car thermal analysis, vol. 1 User Manual, vol. 2 Technical Documentation, Rep. DOT/FRA/ORD-98/09A and 09B, Federal Railroad Administration, U.S. Department of Transportation—DOT, 1998.

- [19] Yu.N. Shebeko, I.A. Bolodian, V.N. Filippov, V.Yu. Navzenya, A.K. Kostyuhin, P.M. Tokarev, E.D. Zamishevski, A study of the behaviour of a protected vessel containing LPG during pool fire engulfment, *J. Hazard. Mater.* A77 (2000) 43–56.
- [20] E. Salzano, B. Picozzi, S. Vaccaro, P. Ciambelli, Hazard of pressurised tanks involved in fires, *Ind. Eng. Chem. Res.* 42 (2003) 1804–1812.
- [21] Y.W. Gong, W.S. Lin, A.Z. Gu, X.S. Lu, A simplified model to predict the thermal response of PLG and its influence on BLEVE, *J. Hazard. Mater.* A108 (2004) 21–26.
- [22] A.M. Birk, Fire Testing and Computer Modelling of Rail Tank-Cars Engulfed in Fires (Literature Review), TP 14561E, 2006.
- [23] C.C. Manu, A.M. Birk, I.Y. Kim, Stress rupture predictions of pressure vessels exposed to fully engulfing and local impingement accidental fire heat loads, *Eng. Failure Anal.* 16 (2009) 1141–1152.
- [24] D.M. Tan, J. Xu, J.E.S. Venart, Fire-induced failure of a propane tank: some lessons to be learnt, *J. Process Mech. Eng. I Mech. E Part E* 217 (2003) 79–91.
- [25] G. Landucci, M. Molag, J. Reinders, V. Cozzani, Experimental and analytical investigation of thermal coating effectiveness for 3 m³ LPG tanks engulfed by fire, *J. Hazard. Mater.* 161 (2009) 1182–1192.
- [26] ANSYS Inc., ANSYSTM User Guide, v.11, 2007.
- [27] J.E.S. Venart, Boiling liquid expanding vapour explosions: possible failure mechanisms and their consequences, in: *ICHEME Hazards XV; Symp. Series 147*, 2000, pp. 121–138.
- [28] American Society of Mechanical Engineers (ASME), Boiler and Pressure Vessel Committee, Boiler and Pressure Vessel code. Section VIII Div. 2, American Society of Mechanical Engineers, New York, 1989.
- [29] G. Landucci, G. Gubinelli, G. Antonioni, V. Cozzani, The assessment of the damage probability of storage tanks in domino events triggered by fire, *Accid. Anal. Prev.*, doi:10.1016/j.aap.2008.05.006, in press.
- [30] M. Molag, J. Reinders, S.J. Elbers, Onderzoek naar de effectiviteit van maatregelen ter voorkoming van een warme BLEVE van een autogas tankauto (in Dutch), Report 2006-A-R0307/B, Netherlands Organisation for Applied Scientific Research—TNO, Apeldoorn, 2006.
- [31] Z. Jin, Y. Asako, Y. Yamaguchi, M. Harada, Fire resistance test for fire protection materials with high water content, *Int. J. Heat Mass Trans.* 43 (2000) 4395–4404.
- [32] J.M. Faucher, D. Giquel, R. Guillemet, J. Kruppa, Y. Le Botlan, Y. Le Duff, H. Londiche, C. Mahier, I. Oghia, J.L. Py, P. Wiedemann, Fire protection study on fire proofing tanks containing pressurized combustible liquefied gases, GEIE (Groupement Européen d'Intérêt Economique) Paris, GASAFE Program Report, Paris, 1993.
- [33] G. Landucci, Development and modelling of passive fire protection systems, Ph.D. Thesis in Chemical Engineering, University of Pisa, Pisa, 2009.
- [34] B. Droste, W. Schoen, Full scale fire tests with unprotected and thermal insulated LPG storage tanks, *J. Hazard. Mater.* 20 (1988) 41–53.
- [35] S.R. Hanna, D.G. Strimaitis, J.C. Chang, Hazard response Modeling uncertainty (a quantitative method), *Sigma Res. Corp. Report*, 1991.
- [36] P.A.M. Uijt de Haag, B.J.M. Ale, Guidelines for Quantitative Risk Assessment, Committee for the Prevention of Disasters, The Hague, 1999 (Purple Book).
- [37] L.T. Cowley, A.D. Johnson, Oil and gas fires—characteristics and impact, OTI 92 596, Health and Safety Executive—HSE, London, 1992.
- [38] T.A. Roberts, I. Buckland, L.C. Shirvill, B.J. Lowesmith, P. Salater, Design and protection of pressure systems to withstand severe fires, *Proc. Saf. Environ. Prot.* 82 (2004) 89–96.
- [39] F.P. Lees, *Loss Prevention in the Process Industries*, second ed., Butterworth-Heinemann, Oxford, 1996.
- [40] T. Cotgreave, Passive fire protection: performance requirements and test methods, OTI Report 92606, prepared by Steel Construction Institute for HSE, London, 1992.